In Situ Raman Spectroscopy of Uranyl Peroxide Nanoscale Cage Clusters Under Hydrothermal Conditions

ARTICLE

In Situ Raman Spectroscopy of Uranyl Peroxide Nanoscale Cage Clusters Under Hydrothermal Conditions

Haylie L. Lobeck,[a] Hrafn Traustason,[b] Patrick A. Julien,[c] John R. FitzPatrick,[a] Sara Mana,[d] Jennifer E.S. Szymanowski,[a] and Peter C. Burns * [a, b]

Aqueous solutions containing the nanoscale uranyl peroxide cage clusters U_{60}, $[(UO_2)(O_2)(OH)]_{60}{}^{60-}$, and $U_{60}Ox_{30}$, $[\{(UO_2)(O_2)\}_{60}(C_2O_4)_{30}]^{60-}$, were monitored by *in situ* Raman spectroscopy during stepwise heating to 180°C. In solutions containing U_{60}, clusters persist to 120°C, although conversion of U_{60} to U_{24}, $[(UO_2)(O_2)(OH)]_{24}{}^{24-}$, occurs above 100°C. $U_{60}Ox_{30}$ persisted in solutions heated to 150°C, although partial conversion to smaller uranyl peroxide clusters species was observed beginning at 100°C. Upon breakdown of the uranyl peroxide cage clusters, uranium precipitated as a compreignacite-like phase, $K_2[(UO_2)_3O_2(OH)_3]_2(H_2O)_7$, and metaschoepite, $[(UO_2)_8O_2(OH)_{12}](H_2O)_{10}$. The role of the countercations, oxalate bridge, and solution pH are examined in order to better understand the mobility of these species at elevated temperatures.

Introduction

Understanding actinide aqueous chemistry is essential for managing nuclear fuel cycles and their potential environmental impact. Under oxidizing conditions, uranium exists as the soluble uranyl ion $(UO_2)^{2+}$.[1] Uranyl ion complexation with peroxide, which is produced by alpha-radiolysis of water,[2] and organics, such as oxalates,[3] is important in the nuclear fuel cycle. Nanoscale cage clusters built from uranyl peroxide polyhedra rapidly self-assemble in alkaline aqueous solutions containing uranyl ions and hydrogen peroxide.[4–6] More than 65 reported uranyl peroxide nanoclusters have diameters ranging from 1.5 to 4 nm and contain from 16 to 124 uranyl ions bridged by peroxide and other linkers including oxalate, pyrophosphate, nitrate, phosphite, iron, and vanadate.[4–6] Actinide materials may interact with water at elevated temperatures during storage of spent nuclear fuel in a geologic repository in which temperatures could exceed 100°C for thousands of years,[7] and in environments where water is used to cool damaged reactor cores during reactor accidents, like at Fukushima-Daiichi.[8, 9]

Extensive studies of the structures and formation of uranyl peroxide cage clusters have been conducted at room temperature,[4] however only two studies have addressed their behaviour at elevated temperatures.[10, 11] In these, U_{40} and U_{50} were crystallized from aqueous solutions that had been heated to 80°C[11] and release of phosphate from $U_{24}Pp_{12}$ (Pp: pyrophosphate) dissolved in water was observed by nuclear magnetic resonance spectroscopy at 70°C.[10] A single study demonstrated persistence of U_{60} to very high pressures.[12] The overall behaviour of uranyl peroxide cage clusters over a range of temperature, pressure, and radiation fields is of interest relative to their potential applications in nuclear fuel cycles.[13–16] Here we investigate the fate of two uranyl peroxide cage clusters dissolved in water at increasing temperatures up to 180°C using *in situ* Raman spectroscopy. Solutions and precipitates resulting from different heat treatments above 80°C were characterized in detail.

The uranyl peroxide nanoclusters studied here are U_{60}, $[(UO_2)(O_2)(OH)]_{60}{}^{60-}$, and $U_{60}Ox_{30}$ (Ox = oxalate), $[\{(UO_2)(O_2)\}_{60}(C_2O_4)_{30}]^{60-}$. Both contain 60 uranyl ions arranged in a fullerene topology identical to that of Buckminsterfullerene C_{60} (Fig. 1).[17–19] Each $(UO_2)^{2+}$ uranyl ion in U_{60} is coordinated by two peroxide and two hydroxyl groups in the equatorial plane of a hexagonal bipyramid (Fig. 1, B).[17, 18] The uranyl ions in $U_{60}Ox_{30}$ are coordinated by two bidentate peroxide groups and one edge-on bidentate oxalate group (Fig. 1, D).[20] K^+ and Li^+ countercations balance the charges of the anionic cages.[17] The K^+ cations are mostly bound to pentagonal windows of the cluster wall and Li^+ cations tend to be disordered and perhaps are mobile in some cluster crystals even at room temperature.[17, 18, 21–23] In solution, some counter cations dissociate from uranyl peroxide cage clusters, yielding clusters with negative charges that are dependent on dissolved cluster concentration.[18, 24, 25] The solubility of salts of U_{60} in water has been measured and is very high, and the persistence of U_{60} in water at ambient temperatures for more than one year has been observed.[4, 22, 24]

a. Department of Civil and Environmental Engineering and Earth Sciences, University of Notre Dame, Notre Dame, IN 46556, USA
b. Department of Chemistry and Biochemistry, University of Notre Dame, Notre Dame, IN 46556, USA
c. Department of Chemistry, McGill University, Montreal, Quebec, Canada H3A 0B8
d. Department of Geological Sciences, Salem State University, Salem, MA 01970, USA

Fig. 1 Polyhedral configuration and uranyl ion units of U_{60} (A, B) and $U_{60}Ox_{30}$ (C, D) clusters. Uranium = yellow, oxygen = red, and carbon = black.

Experimental Section

Synthesis of U_{60} and $U_{60}Ox_{30}$

Crystals containing U_{60}, $Li_{44}K_{16}[(UO_2)(O_2)(OH)]_{60} \cdot nH_2O$, were synthesized using previously established methods.[17, 21] In a 20 mL scintillation vial, 1 mL of a 0.5 M $(UO_2)(NO_3)_2(H_2O)_6$ aqueous solution was combined with 250 µL of a 0.4 M KCl solution. While stirring, 1 mL of 30% H_2O_2 was added, followed by 750 µL of a 2.38 M LiOH solution in 50 µL aliquots. The resulting clear yellow solution had a pH of ~ 9.3. The vial was left uncovered for two weeks, during which diffraction quality crystals formed during slow evaporation of the solvent.

Crystals containing $U_{60}Ox_{30}$, $Li_{12}K_{48}[\{(UO_2)(O_2)\}_{60}(C_2O_4)_{30}] \cdot nH_2O$, were prepared by combining 100 µL of a 0.5 M $(UO_2)(NO_3)_2(H_2O)_6$ aqueous solution with 100 µL of 30% H_2O_2, followed by 100 µL of a 2.38 M solution of LiOH in a 5 mL vial. Once bubbling had stopped, 50 µL of 0.5 M oxalic acid was added to the vial followed by 400 µL of 0.25 M aqueous potassium hydrogen phthalate solution. The vial was covered with parafilm with a few small holes to allow slow evaporation. Diffraction quality single crystals began forming after two weeks.

The nanocluster crystals were harvested from their mother solutions by vacuum filtration and rinsed lightly using ultrapure (18 MΩ) water. The crystals were subsequently dissolved in ultrapure water to make 30 mg mL^{-1} cluster solutions. A new solution was made for each trial performed to ensure solution age was constant.

Synthesis of Compreignacite

Compreignacite, $K_2[(UO_2)_3O_2(OH)_3]_2(H_2O)_7$, was prepared using previously published methods.[26] In a 23 mL Teflon – lined stainless steel Parr reaction vessel, 0.21 g $UO_2(CH_3COO)_2(H_2O)_2$ and 0.03 g K_2CO_3 were combined with 5 mL of ultrapure water. The pH of the solution was adjusted to ~5 using dilute solutions of KOH or HCl, and heated to 100°C in a Fisher Scientific Isotemp

oven for 24 hours. After cooling to room temperature, the precipitate was recovered by vacuum filtration and thoroughly washed twice with ultrapure water. Powder X-ray diffraction data (see below) confirmed the purity of the compreignacite (Fig. S1).

In Situ Raman Spectroscopy

A 2 mL aliquot of a 30 mg mL^{-1} U_{60} or $U_{60}Ox_{30}$ solution was added to a custom-built 4 mL sapphire vial (Rayotek Scientific, Inc.) (Fig. S2). A custom-built Teflon stopper was secured to the tube using a wire and clamp to ensure the vessel would remain sealed during the heating experiment. The sapphire vial was placed into a custom-built Parr reaction vessel equipped with temperature and pressure probes and two sapphire windows (Fig. 2). A heating jacket was wrapped around the Parr vessel and temperature was controlled by a Parr 4838 heater. A Raman probe was positioned near one of the sapphire windows aligned with the sample vial. The vessel was slowly heated from 30°C to 180°C in a stepwise fashion over the course of 61 hours (Fig. S3). The temperature inside the vessel was measured by a thermocouple every 30 seconds and recorded and Raman spectra were collected every thirty minutes over the duration of the experiment. Each 10°C temperature increment between 60°C and 180°C was maintained for three hours to ensure that a representative series of Raman spectra were collected at each temperature. Solution pH was recorded prior to and after heating. Solutions and solids recovered at room temperature after the heating experiment were analysed as described below.

Raman data was collected using a Bruker Sentinel system equipped with a fibre optic probe, thermoelectric cooled CCD detector, and a 785 nm excitation source. Spectra were collected over the range of 80 – 3200 cm^{-1} using ten 60-second exposures at 400 mW laser power. Baseline corrections were
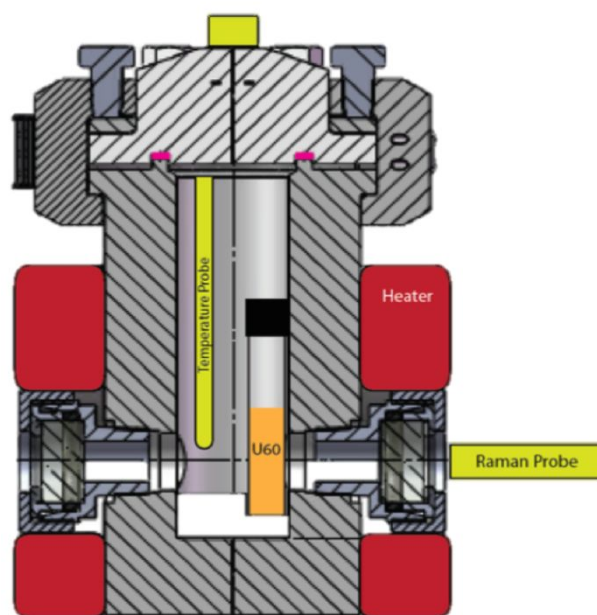
Fig. 2 Schematic of the custom Parr reaction vessel equipped with sapphire windows used in the *in situ* heating experiment.

ARTICLE

performed on each data set using the Sonneveld and Visser algorithm implemented in MATLAB.[27]

Oven Experiments

To better characterize the solutions and solids that resulted from heating to each soak point studied by *in situ* Raman spectroscopy, multiple experiments were conducted in which 2 mL of a 30 mg mL^{-1} U$_{60}$ or U$_{60}$Ox$_{30}$ solution was added to a 23 mL Teflon-lined Parr reaction vessel and was subsequently heated in a Fisher Scientific Isotemp oven from 30°C to the specified soak temperature between 80°C and 180°C at a rate of 0.1°C min^{-1}. The reactions were held at the soak temperature for three hours, then the vessels were allowed to cool to room temperature before the products were removed and separated by centrifugation. The pH of the solution was recorded and any precipitate formed was rinsed twice with ultrapure water and left on the benchtop to dry.

Inductively Coupled Plasma – Optical Emission Spectrometry (ICP-OES)

Elemental analyses were performed using a Perkin Elmer Avio 200 Inductively Coupled Plasma Optical Emission Spectrometer (ICP-OES). Solid samples were prepared by dissolving 2 mg of solid in 1 mL of 5% HNO$_3$. The solutions were further diluted in a 5% HNO$_3$ matrix for analysis. Solution samples were prepared by diluting aliquots of each reaction solution in a 5% HNO$_3$ matrix. Ten calibration standards were prepared with U concentrations from 0.01 to 40 ppm, Li concentrations from 1 to 5 ppm, and K concentrations from 0.1 to 9 ppm. An internal standard of 0.5 ppm Y was added to each standard, sample, and blank to monitor for instrumental drift. Uncertainties reported are derived from the standard deviation of replicate reactions.

Powder X-Ray Diffraction (PXRD)

Powder X-ray diffraction (PXRD) measurements were conducted on a Bruker D8 Davinci diffractometer equipped with CuKα radiation and a solid-state detector. Samples were prepared by dry mounting approximately 10 mg of finely ground powder on a zero-background oriented quartz slide. Patterns were collected using a sample rotation speed of 15°m^{-1}, a 2θ range from 5 - 55°, a step size of 0.01°, and a scan rate of 1.0 second per step.

Electrospray Ionization Mass Spectrometry (ESI-MS)

Electrospray ionization mass spectra (ESI-MS) were acquired using a Bruker Compact QqTOF high-resolution mass spectrometer in negative ion mode (3800 V capillary voltage, an endplate offset of -500 V, 0.8 bar nebulizer gas, 4.0 L min^{-1} dry gas, 180°C dry gas temperature). Samples were diluted to a uranium concentration less than 100 ppm and were introduced into the spectrometer by direct injection at a rate of 180 μL hr^{-1}. Spectra were collected over a 500-5000 m/z range with data averaged over five minutes. Data deconvolution was performed

using the MaxEnt feature of the Bruker DataCompass data-analysis software.

Scanning Electron Microscopy (SEM)

Secondary electron images were collected on a JEOL JCM-6000Plus scanning electron microscope (SEM). Images were collected under high vacuum using 10kV accelerating voltage and a 50 pA probe current at x4000 magnification. Samples were pressed onto double-sided carbon tape and mounted on a 12.7 mm aluminium SEM stub.

Results

In Situ Raman Spectroscopy of U$_{60}$ in Water Heated to 180°C

In situ Raman spectroscopy provides insights into the local bonding environments of uranyl peroxide species in solution as they are heated. U$_{60}$ in solution has two Raman active bands at 804 cm^{-1} and 842 cm^{-1}, assigned to the symmetric stretch of the uranyl, v_s(UO$_2$)$^{2+}$, and the second vibrational mode of bound peroxide, v_2(O$_2$)$^{2-}$, respectively.[12] Fig. 3 illustrates 128 Raman spectra of a 30 mg mL^{-1} U$_{60}$ solution heated stepwise from room temperature to 180°C over 61 hours. Bands at 378 cm^{-1}, 417 cm^{-1}, 429 cm^{-1}, 448 cm^{-1}, 576 cm^{-1}, 644 cm^{-1}, and 749 cm^{-1} are Raman active signals of the sapphire vessel and windows of the heating apparatus.[28, 29] Previous studies[28, 30] have found that there is a known temperature – dependent shift of Raman Stokes and anti-Stokes peaks in the sapphire spectrum. As temperature increases, the bond lengths within the sapphire crystal lattice change, which result in an observed red shift of the Stokes peaks.[28, 31] In this experiment, a red shift from 417 cm^{-1} to 414 cm^{-1} was observed for the most intense sapphire peak between spectra taken at room temperature versus spectra acquired at 180°C (Fig. S4). In order to normalize to temperature and better interpret the uranyl peroxide nanocluster data, each spectrum collected was shifted and centred relative to the 417 cm^{-1} sapphire signal.

The Raman band at ~842 cm^{-1} is assigned to peroxide that bridges two uranyl ions, with the peroxide bidentate to each uranyl ion. Although some uranyl species other than uranyl peroxide cage clusters contain similar peroxide environments, loss of this signal in the current case indicates that the uranyl peroxide cage cluster has decomposed. The band due to uranyl will persist in the Raman spectra unless reduction occurs, although the mode is expected to shift if the bonding environment changes.[32] The v_2(O$_2$)$^{2-}$ band of aqueous U$_{60}$ at 842 cm^{-1} is unchanged during heating from 30°C to 100°C. Between 110°C to 120°C, the band begins to broaden and weaken, and by 130°C the signal is lost (Fig. 4). A blue shift of the uranyl band from 804 cm^{-1} to 812 cm^{-1} begins at 110°C (Fig. 4) and indicates shortening of the O=U=O bond lengths.[32, 33] Raman spectra collected for solutions at 130°C to 180°C (Fig. 3) are very similar.

U$_{60}$ persists up to 100°C in solution, begins to decompose by 110°C, and is destroyed by 130°C. The breakdown products of U$_{60}$ present at 120°C appear unchanged up to 180°C and through cooling to room temperature.
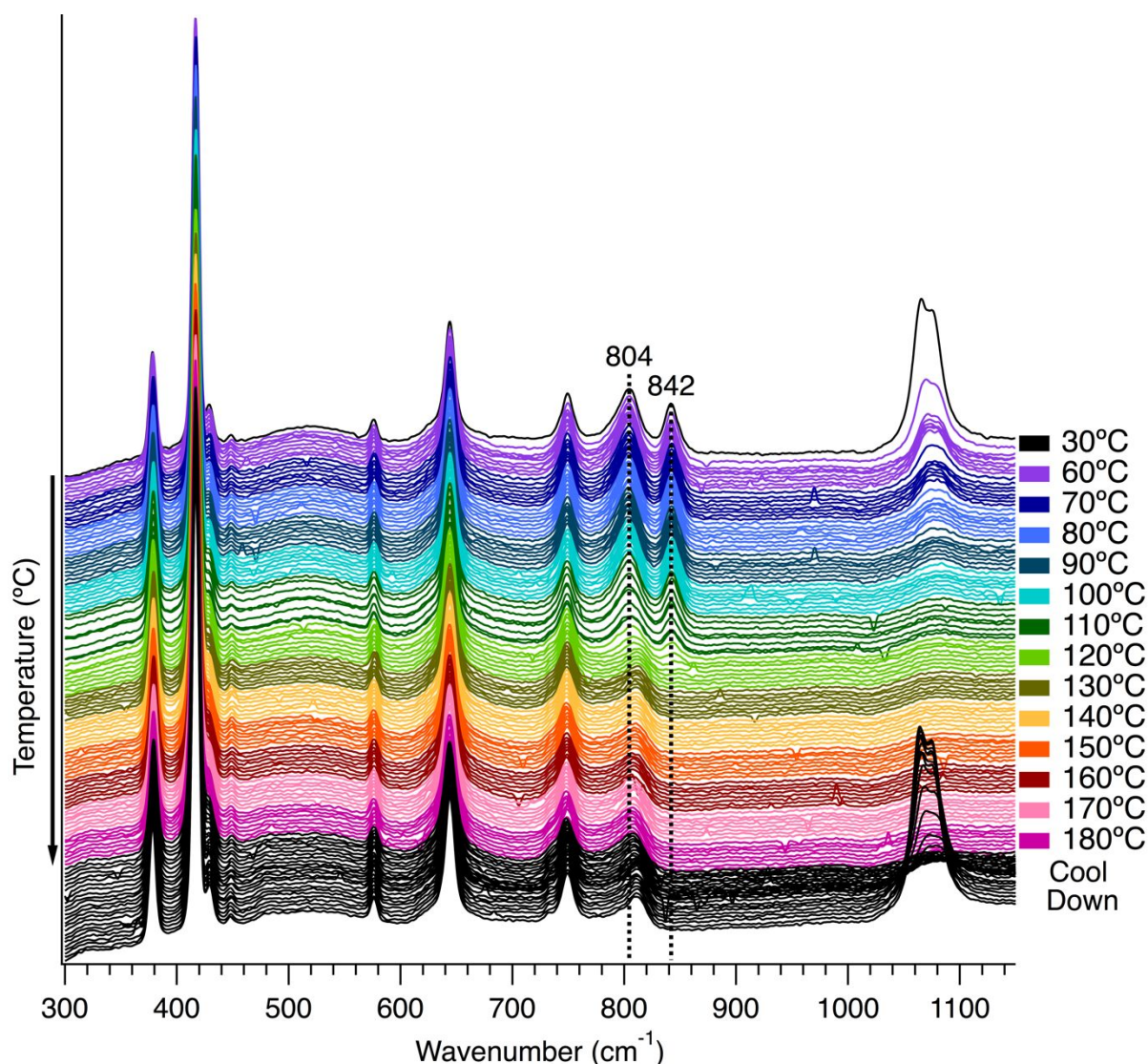
Fig. 3 Colour graph composed of *in situ* Raman spectra collected of a U_{60} solution heated to 180°C.
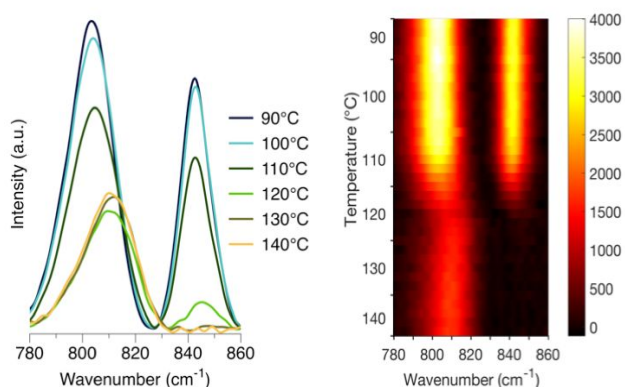
Fig. 4 Averaged Raman spectra of U_{60} solution at temperatures between 90°C and 140°C (left) and overhead view of Raman spectra between 780 and 860 cm^{-1} as temperature increases (right).

Characterization of U_{60} Solutions

Elemental analyses of heated U_{60} solutions are summarized in Fig. 5. The concentration of each element in solution was measured before and after the heating cycle in the oven and results are displayed as the percentage of each element remaining in solution at each temperature. Elemental concentrations in U_{60} solutions heated to 80°C through 100 °C are similar to those of unheated solutions. Upon heating to 110°C a visible precipitate forms, and the solution uranium concentration drops to ~10% of the original concentration. Potassium and lithium concentrations in solution decrease to roughly half of their original concentrations. For solutions heated to 120°C, most of the uranium has precipitated, and lithium and potassium concentrations remain at half of their original concentrations. For solutions heated between 130°C and 180°C, uranium and potassium concentrations approach zero, and lithium concentrations remain steady at ~40% of the original concentration. The pH of the original U_{60} solutions was 10.17 ± 0.47. U_{60} solutions heated between 80°C and 100°C had a measured pH of 10.77 ± 0.51 upon cooling, and the pH of
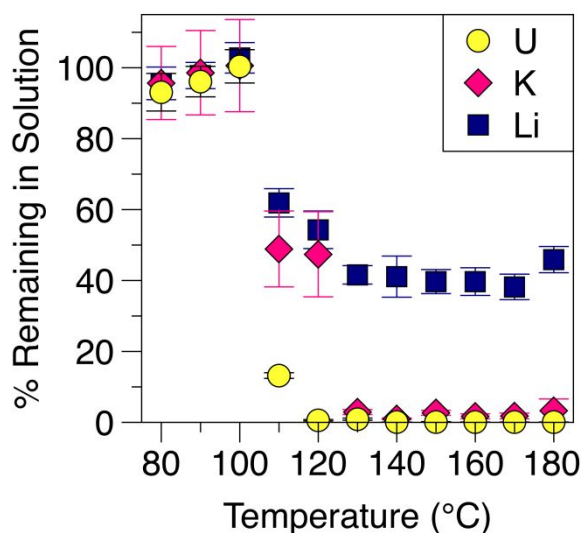
Fig. 5 Elemental analyses of 30 mg mL^{-1} U$_{60}$ solutions after being heated to temperatures between 80°C and 180°C.

solutions heated between 110°C and 180°C increased, and was measured to be 12.09 ± 0.30 upon cooling.

ESI-MS data for heated solutions that initially contained U$_{60}$ are shown in Fig. 6. Solutions containing U$_{60}$ produce broad signals centred at 1820, 1980, and 2190 m/z and are highlighted in red. Charges of -12, -11, and -10 are assigned to the respective signals, and are consistent with a single 20.4 kDa species in solution. At 100°C, in addition to U$_{60}$, a smaller cluster species is detected with MS signals at 1340, 1620, and 2040 m/z (highlighted in blue). Charges of -6, -5, and -4 were assigned to these signals and are consistent with a uranyl peroxide cluster with an average mass of 8.3 kDa, likely U$_{24}$, [(UO$_2$)(O$_2$)(OH)]$_{24}$$^{24-}$.[34, 35] Spectra of solutions heated between 110°C and 130°C indicate U$_{24}$ as the only cluster in solution, and solutions heated at and above 140°C contain no cluster signals (Fig. 6).

Replacement of U$_{60}$ by U$_{24}$ in solution upon heating between 100 and 120°C is accompanied by blue shifts of the uranyl (804 to 810 cm^{-1}) and bound peroxide (842 to 845 cm^{-1}) bands in the Raman spectra (Fig. 4). Previously reported Raman data of solutions of U$_{24}$ contain signals for v_s(UO$_2$)$^{2+}$ and v_2(O$_2$)$^{2-}$ at 810 cm^{-1} and 847 cm^{-1}.[35, 36] For solutions heated above 130°C, the signal from bound peroxide is no longer detected, and uranyl signals in the Raman spectra are attributed to the precipitate formed.

Characterization of Solid Phases

Powder X-ray diffraction indicates the same canary yellow microcrystalline precipitate forms from all solutions of U$_{60}$ heated above 120°C (Fig. S5), and its diffraction pattern is compared with those of known uranyl oxide hydroxy-hydrate phases in Fig. 7. The observed pattern is similar to those of schoepite, [(UO$_2$)$_8$O$_2$(OH)$_{12}$](H$_2$O)$_{12}$, metaschoepite, [(UO$_2$)$_8$O$_2$(OH)$_{12}$](H$_2$O)$_{10}$, leesite, K[(UO$_2$)$_4$O$_2$(OH)$_5$](H$_2$O)$_5$, and compreignacite, K$_2$[(UO$_2$)$_3$O$_2$(OH)$_3$]$_2$(H$_2$O)$_7$.[26, 37 – 39] SEM images of the precipitate and synthetic compreignacite reveal similar microcrystalline morphologies (Fig. 8, S6). Both materials are
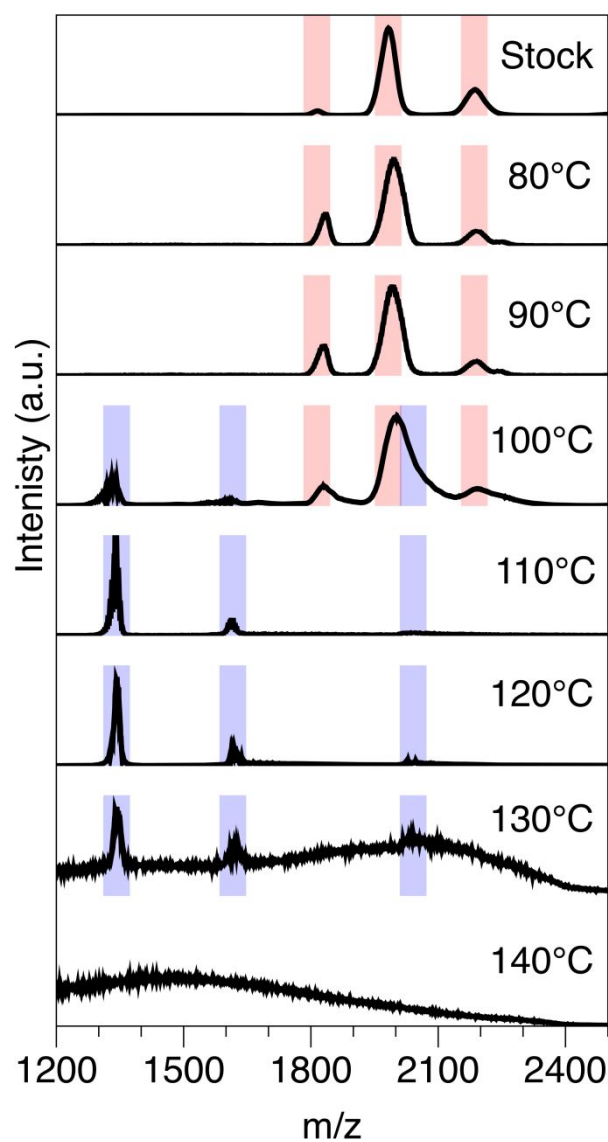
Fig. 6 ESI-MS spectra of a U$_{60}$ solution heated between 80°C and 140°C. Bands highlighted in red at 1820, 1980, and 2190 m/z are assigned charges of -12, -11, and -10, respectively, and correspond to U$_{60}$ in solution. Bands highlighted in blue at 1340, 1620, and 2040 m/z are assigned charges of -6, -5, and -4, respectively, and correspond to U$_{24}$ in solution.
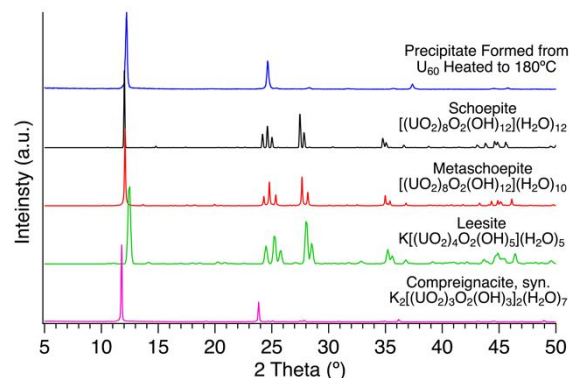
Fig. 7 PXRD patterns of solid formed from heating a U$_{60}$ solution to 180°C versus known uranyl oxide hydroxy-hydrate mineral phases schoepite (COD # 9004444), metaschoepite (COD # 9010196), leesite (simulated pattern)[39], and synthetic compreignacite.
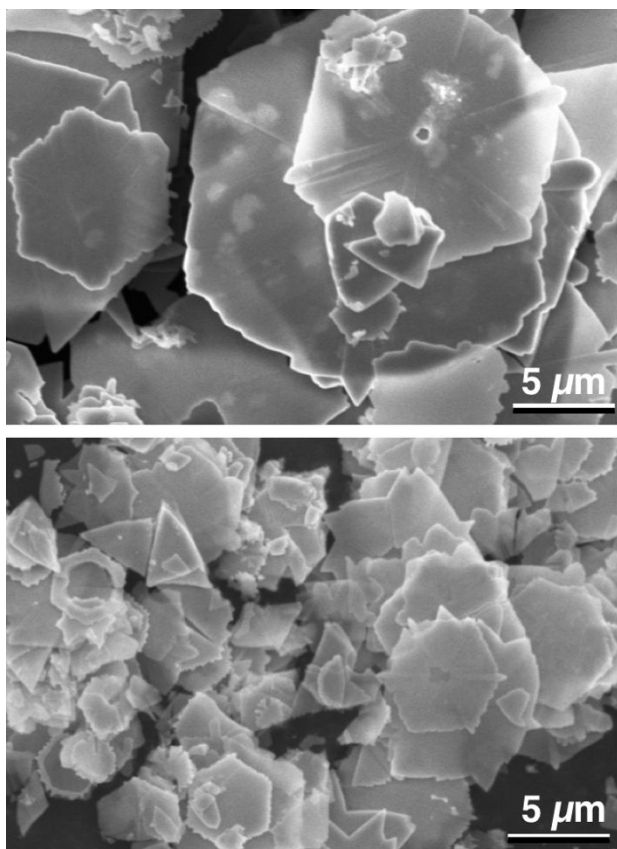
Fig. 8 SEM images of solid formed from heating a U_{60} solution to 180°C (top) and synthetic compreignacite (bottom) at x4000 magnification.

composed of 5 – 20 μm subhedral hexagonal and triangular plates. Elemental analysis of the precipitate and synthetic compreignacite along with the calculated weight percent of each element in the known phases are presented in Table 1. The composition of the precipitate is similar to compreignacite, potassium uranyl-oxide hydroxy-hydrate, perhaps with some incorporation of Li in the interlayer.

In Situ Raman Spectroscopy of $U_{60}Ox_{30}$ in Water Heated to 180°C

An aqueous solution containing 30 mg mL^{-1} $U_{60}Ox_{30}$ produces three Raman bands at room temperature. The bands at 816 cm^{-1} and 832 cm^{-1} are assigned as the symmetric stretch of the uranyl ion $v_s(UO_2)^{2+}$ and the second vibrational mode of the bound peroxide $v_2(O_2)^{2-}$, respectively. The band at 846 cm^{-1} is similar to those in spectra of aqueous uranyl oxalate

complexes,[40, 41] and is assigned here to the uranyl-oxalate bridges within the nanocluster. Fig. 9 illustrates 130 Raman spectra collected for a 30 mg mL^{-1} $U_{60}Ox_{30}$ solution heated stepwise from room temperature to 180°C over 61 hours (Fig. S3). The bound peroxide and oxalate signals at 832 cm^{-1} or 846 cm^{-1} are indicative of the nanocluster, and the uranyl ion band at 816 cm^{-1} is expected to persist and red or blue shift upon cluster breakdown.[32, 40, 41] Upon heating, all three of these Raman bands decrease in intensity (Fig. 10). Between 140°C and 150°C, the peroxo and oxalate bands are slightly red shifted and disappear by 160°C, and the uranyl band shifts from 816 cm^{-1} to 821 cm^{-1} due to shortening of the O=U=O uranyl bonds. The Raman spectra collected for solutions and solids resulting from the decomposition of $U_{60}Ox_{30}$ (Fig. 9) remain mostly unchanged between 160°C to 180°C and upon cooling to room temperature.

Characterization of $U_{60}Ox_{30}$ Solutions

Heating experiments, similar to those described above for U_{60} solutions, were performed by heating a 30 mg mL^{-1} $U_{60}Ox_{30}$ solution in an oven at 0.1°C min^{-1} to between 100°C and 180°C. Solutions were soaked at target temperatures for three hours. Elemental analyses of the resulting $U_{60}Ox_{30}$ solutions are reported in Fig. 11. The compositions of $U_{60}Ox_{30}$ solutions heated to 140°C remain constant. At 150°C, ~20% of the original uranium remains in solution and both potassium and lithium concentrations are ~60% of their original concentrations. By 180°C, ~10% of the original uranium remains in solution, while potassium and lithium remain at ~60% of their original concentration. The average initial and final pH values of the reaction solutions were 7.11 ± 0.17 and 6.63 ± 0.35, respectively.

ESI-MS of a $U_{60}Ox_{30}$ solution heated to between 100°C and 180°C are shown in Fig. 12. Unheated solutions of $U_{60}Ox_{30}$ produce five broad signals at 1540, 1710, 1880, 2050, and 2250 m/z. These correspond to charges of -13 to -9 and yield an average mass of 21.0 kDa. The $U_{60}Ox_{30}$ MS signals persist for solutions heated to 150°C, and are absent for solutions heated at 160°C. Broad MS signals at 1660, 1820, 1970, 2010, and 2150 m/z are produced by solutions heated between 100°C and 150°C, and are taken to indicate a mixture of smaller species ranging between 9.3 kDa and 18.9 kDa.

Table 1 Elemental compositions of unknown precipitate and known uranyl oxide hydroxy-hydrate mineral phases.

Phase	Chemical Formula	wt. % U	wt. % K	wt. % Li	wt. % O	References
Unknown Phase	-	70.3 ± 6.6	4.8 ± 2.8	0.7 ± 0.2	-	Measured*, this work
Schoepite	$[(UO_2)_8O_2(OH)_{12}](H_2O)_{12}$	72.9	-	-	25.7	Calculated[26]
Metaschoepite	$[(UO_2)_8O_2(OH)_{12}](H_2O)_{10}$	73.9	-	-	24.8	Calculated[26, 38]
Leesite	$K[(UO_2)_4O_2(OH)_5](H_2O)_5$	71.8	3.0	-	24.1	Calculated[37, 39]
Compreignacite	$K_2[(UO_2)_3O_2(OH)_3]_2(H_2O)_7$	71.8	3.9	-	23.3	Calculated[26, 37]
Compreignacite, syn.	$K_2[(UO_2)_3O_2(OH)_3]_2(H_2O)_7$	71.8 ± 2.5	4.6 ± 1.0	-	-	Measured*, this work

*Measured by ICP-OES
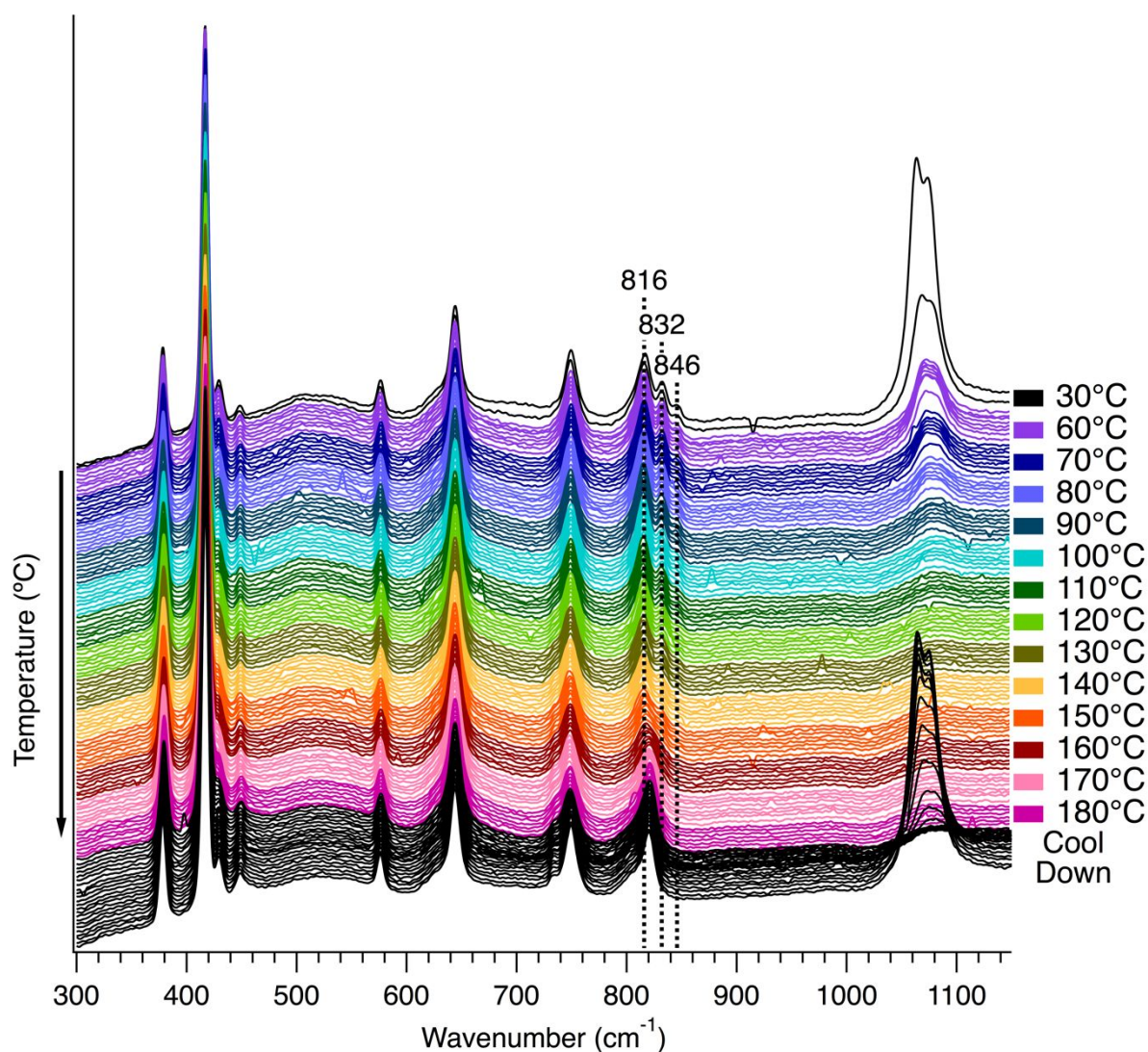
Fig. 9 Colour graph composed of *in situ* Raman spectra collected of a $U_{60}Ox_{30}$ solution heated to 180°C.
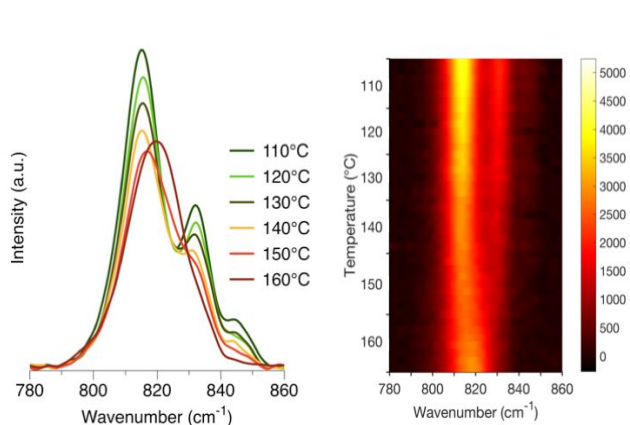
Fig. 10 Averaged Raman spectra of $U_{60}Ox_{30}$ solution at temperatures between 110°C and 160°C (left) and overhead view of Raman spectra between 780 and 860 cm^{-1} as temperature increases (right).
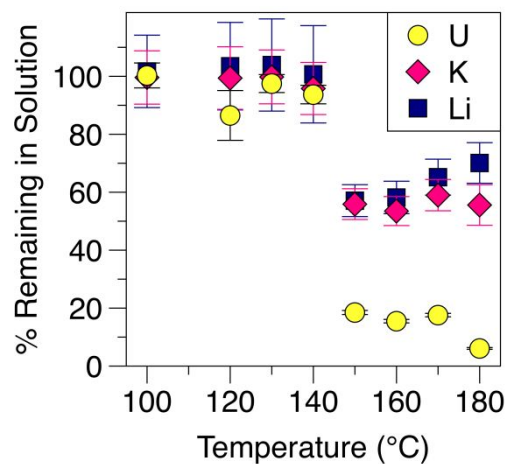
Fig. 11 Elemental analyses of 30 mg mL^{-1} $U_{60}Ox_{30}$ solutions after being heated to temperatures between 100°C and 180°C.

Journal Name
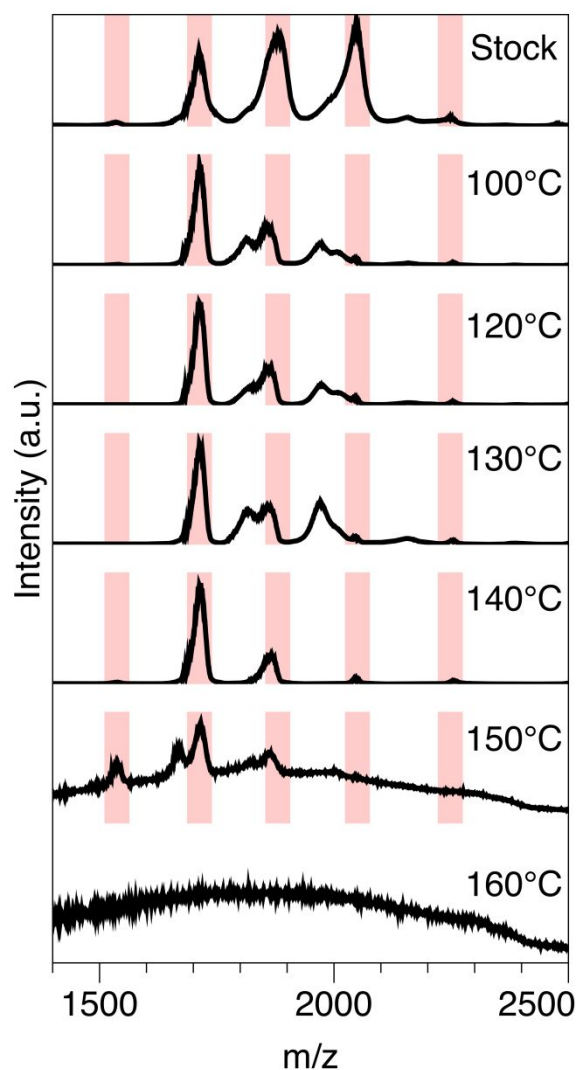
Fig. 12 ESI-MS spectra of a $U_{60}Ox_{30}$ solution heated between 100°C and 160°C. Bands highlighted in red at 1540, 1710, 1880, 2050, and 2250 m/z are assigned charges of -13, -12, -11, -10, and -9 respectively, and correspond to $U_{60}Ox_{30}$ in solution.

ICP-OES and ESI-MS data indicate that some $U_{60}Ox_{30}$ clusters remain intact through heating to 150°C and a mixture of smaller cluster species form and are detected upon the partial breakdown of the $U_{60}Ox_{30}$ cluster. No nanoclusters are present in solution above 160°C, although reaction solutions still contain 10% of the original uranium as smaller aqueous species.
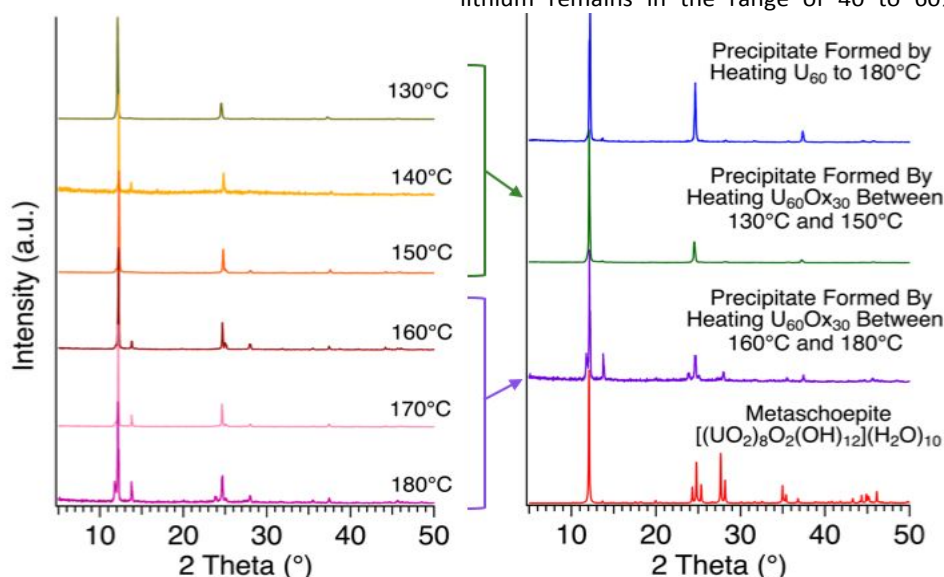
Characterization of Solid Phases

As for U_{60} solutions described above, PXRD indicates that the canary yellow microcrystalline precipitate formed in solutions containing $U_{60}Ox_{30}$ heated above 130°C are the same compreignacite-like material (Fig. 13). Metaschoepite, $[(UO_2)_8O_2(OH)_{12}](H_2O)_{10}$, is also precipitated from $U_{60}Ox_{30}$ solutions heated between 160°C and 180°C. The precipitate formed from the decomposition of $U_{60}Ox_{30}$ contains 67.5 ± 3.1 wt. % U, 1.7 ± 0.8 wt. % K, and 0.6 ± 0.1 wt. % Li, and is a mixture of materials (Fig. 14, S7). Hexagonal and triangular plate-like crystals, similar to those in found in the U_{60} system (Fig. 8), ranging in size from 5 − 30 μm were observed for solutions heated above 130°C, and the second phase has an acicular morphology in the $U_{60}Ox_{30}$ system.

Discussion

An *in situ* Raman spectroscopy technique was implemented to probe the persistence of two uranyl peroxide nanoclusters in aqueous solutions heated stepwise to 180°C. Each cluster was exposed to the same temperature and pressure conditions inside the heating vessel, so the differences observed between the U_{60} and $U_{60}Ox_{30}$ systems at each temperature can be attributed to factors including countercation effects, solution pH, and the behaviour of the bridging peroxide and oxalate ligands on the clusters at elevated temperatures. In the solid state, U_{60} can withstand pressures approaching 17.4 GPa,[12] which are dramatically higher than the pressure of ~0.001 GPa for solutions at 180°C in the current experiments. Changes of the properties of water including reduction of the dielectric constant, an increased ion product, and reduced hydrogen bonding occur for temperatures approaching 200°C[42] and may influence the stability and reactivity of uranyl nanoclusters.

The counter cations in salts of both U_{60} and $U_{60}Ox_{30}$ are Li^{+} and K^{+}. Elemental analysis of each 30 mg mL^{-1} stock solution studied here produced molar ratios of 60 U: 24 ± 2 K: 43 ± 1 Li (U_{60}) and 60 U: 45 ± 4 K: 12 ± 2 Li ($U_{60}Ox_{30}$). Counter cations associated with uranyl clusters impact the solubility and aggregation of uranyl peroxide nanoclusters in solution.[18, 21, 25, 34, 43] Counter cations with larger hydrated radii (Na^{+} and Li^{+}) do not associate as strongly with the anionic cage clusters in solution as K^{+} and Cs^{+}.[4] After U_{60} and $U_{60}Ox_{30}$ clusters break down in solution upon heating in the current experiments, lithium remains in the range of 40 to 60% of its original

Fig. 13 PXRD patterns collected of solids formed from a $U_{60}Ox_{30}$ solution heated between 130°C and 180°C (left). Comparison of PXRD patterns from solid formed between the U_{60} heating reactions, $U_{60}Ox_{30}$ heating reactions, and metaschoepite (COD # 9010196) (right).
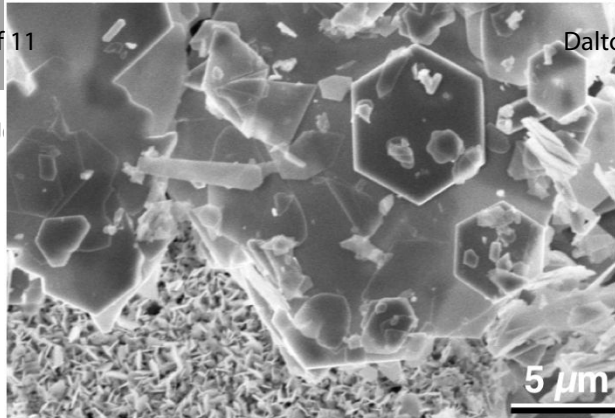
Fig. 14 SEM image of solid formed from heating a $U_{60}Ox_{30}$ solution to 160°C at x4000 magnification.

concentration in solution (Fig. 5 and 11). For solutions containing U_{60} above 130°C, K^+ and U are precipitated into a compreignacite-like phase. A similar phase is formed from solutions containing $U_{60}Ox_{30}$, although some of the clusters remain intact until above 150°C. At this temperature, most of the uranium and 50% of the original potassium in solution precipitates. The $U_{60}Ox_{30}$ solution contains nearly double the amount of K^+ with respect to U as that of U_{60}, and formation of a compreignacite-like compound requires only half of the original K^+ of the $U_{60}Ox_{30}$ solution. The presence of more K^+ in the $U_{60}Ox_{30}$ system may help stabilize the nanocluster and allowed it to persist to temperatures 40°C higher in solution relative to U_{60}. At lower temperatures, K^+ cations are bonded to the cage clusters inside the five-membered rings.[17]

The oxalate groups that bridge uranyl ions may help to stabilize $U_{60}Ox_{30}$ to higher temperatures than U_{60}. Di Bernardo et al.[6] investigated the aqueous complexation of the uranyl ion to oxalate and found that as the temperature of the solution increased from 30°C to 70°C, the uranyl oxalate complexes became more thermodynamically stable due to their increasing positive entropies of complexation. While current thermodynamic studies of uranyl peroxide cage clusters do not include $U_{60}Ox_{30}$,[4, 44] future calorimetric work could provide valuable insight on the heats of formation of this cluster compared to U_{60}.

Beyond the intrinsic stability and dynamics of the clusters themselves, the degradation of clusters has a significant effect on the solution environment. The pH of each experiment was measured before heating and upon cool down for each U60 and U60Ox30 solution. An unheated aqueous solution of U60 had a pH of ~10, where solutions heated between 80°C and 100°C had pH values of ~11 after cooling. The measured final pH values of U60 solutions heated at and above 110°C increased to ~12. Interestingly, in the $U_{60}Ox_{30}$ systems, the pH remained at ~7 for both unheated solutions and final solutions of experiments heated up to 180°C. Oxalate is a weak base and tends to form strong chelating complexes with uranyl.[3] Oxalic acid is often used to stabilize pH in the synthesis of uranyl peroxide clusters,[45, 46] and could also stabilize the pH in the heated aqueous solution of $U_{60}Ox_{30}$. The U_{60} system lacks such a buffer, and this may result in the cluster destruction observed at lower temperatures. Both the U_{60} and $U_{60}Ox_{30}$ stock solutions were prepared under ambient conditions, so further pH change in the systems could occur from reactions between water and carbon dioxide in the atmosphere. Raman bands in the 1063 cm^{-1} to 1073 cm^{-1} region were detected in both cluster solutions at room temperature and are attributable to the symmetric

stretch of free carbonate in solution, $v_1(CO_3)^{2-}$ (Fig. 3 and 9).[47] The free carbonate signals decreased for heated solutions and were absent from the spectra collected between 120°C and 180°C before returning upon cooling the reaction. Upon heating, the free carbonate in solution is converted to $CO_{2(g)}$ and moves to the headspace of the reaction vessel.[48] Since the vessel is sealed, the $CO_{2(g)}$ remains in the system, and once cooled, the carbonate returns to solution to restore equilibrium. Carbonate may therefore impact the pH and speciation of uranyl in solution.

The observation that U_{60} is replaced by U_{24} and a partial conversion of $U_{60}Ox_{30}$ to smaller species upon heating the cluster-bearing solutions to 100°C (Fig. 6 and 12) suggests that further *in situ* Raman and thermodynamic studies on heating uranyl peroxide nanoclusters could illuminate the speciation and reactivity of clusters and provide insight on how cluster topology relates to stability.

Conclusions

Uranyl peroxide nanoclusters have been studied experimentally,[21, 24, 49, 50] computationally,[21, 25, 51 – 53] and thermodynamically,[44, 54] though information on their behaviours in solution at elevated temperatures is currently lacking. This study investigated the behaviours of two nanoclusters, U_{60} and $U_{60}Ox_{30}$, in aqueous solutions heated to 180°C. Under similar heating conditions, $U_{60}Ox_{30}$ persists in water at temperatures 40°C greater than U_{60}. The role of the countercations, oxalate bridges, and solution pH may be important for the stability of uranyl peroxide nanoclusters in solution at elevated temperatures. Both oxalate and peroxide are relevant in the production of plutonium and uranium oxide precursors for the fabrication of mixed-oxide fuels (MOX).[14, 55] Understanding the behaviour of uranyl peroxo and peroxo-oxalate clusters in aqueous solutions at relevant temperatures is important in determining their potential role in the fuel cycle.

Conflicts of interest

There are no conflicts to declare.

Acknowledgements

References

1   R.J. Finch and R.C. Ewing, *J. Nucl. Mater.*, 1992, **190**, 133-156.

2   G. Sattonnay, C. Ardois, C. Corbel, J.F. Lucchini, M.F. Barthe, F. Garrido, and D. Gosset, *J. Nucl. Mater.*, 2001, **288**, 11-19.

3   P. Di Bernardo, P.L. Zanonato, G.X. Tian, M. Tolazzi, and L.F. Rao, *Dalton Trans.*, 2009, **23**, 4450-4457.

4   P.C. Burns and M. Nyman, *Dalton Trans.* 2018, **47**, 5916-5927.

5   P.C. Burns, *Mineral. Mag.,* 2011, **75**, 1-25.

6   J. Qiu and P.C. Burns, *Chem. Rev.,* 2013, **113**, 1097-1120.

7   J.C.S. Long and R.C. Ewing, *Annu. Rev. Earth Planet. Sci.*, 2004, **32**, 363-401.

8   B. Grambow and C. Poinssot, *Elements*, 2012, **8**, 213-219.

9   C.R. Armstrong, M. Nyman, T. Shvareva, G.E. Sigmon, P.C. Burns and A. Navrotsky, *Proc. Natl. Acad. Sci. of the U. S. A.,* 2012, **109**, 1874-1877.

10   R.L. Johnson, C.A. Ohlin, K. Pellegrini, P.C. Burns and W.H. Casey, *Angew. Chem., Int. Ed.*, 2013, **52**, 7464-7467.

11   T.Z. Forbes, J.G. McAlpin, R. Murphy and P.C. Burns, *Angew. Chem., Int. Ed.*, 2008, **47**, 2824-2827.

12   K.M. Turner, J.E.S. Szymanowski, F.X. Zhang, Y. Lin, B.T. McGrail, W.L. Mao, P.C. Burns and R.C. Ewing, *J. Mater. Res.*, 2017, **32**, 3679-3688.

13   F. Blanchard, M. Ellart, M. Rivenet, N. Vigier, I. Hablot, B. Morel, S. Grandjean and F. Abraham, *Chem. Commun.*, 2016, **52**, 3947-3950.

14   F. Blanchard, M. Ellart, M. Rivenet, N. Vigier, I. Hablot, B. Morel, S. Grandjean and F. Abraham, *Cryst. Growth Des.*, 2016, **16**, 200-209.

15   E.M. Wylie, K.M. Peruski, S.E. Prizio, A.N.A. Bridges, T.S. Rudisill, D.T. Hobbs, W.A. Phillip and P.C. Burns, *J. Nucl. Mater.*, 2016, **473**, 125-130.

16   E.M. Wylie, K.M. Peruski, J.L. Weidman, W.A. Phillip, and P.C. Burns, *ACS Appl. Mater. Interfaces*, 2014, **6**, 473-479.

17   T.A. Olds, M. Dembowski, X.P. Wang, C. Hoffman, T.M. Alam, S. Hickam, K.L. Pellegrini, J.H. He and P.C. Burns, *Inorg. Chem.*, 2017, **56**, 9676-9683.

18   L.R. Sadergaski, W. Stoxen and A.E. Hixon, *Environ. Sci. Technol.*, 2018, **52**, 3304-3311.

19   G.E. Sigmon, D.K. Unruh, J. Ling, B. Weaver, M. Ward, L. Pressprich, A. Simonetti and P.C. Burns, *Angew. Chem., Int. Ed.*, 2009, **48**, 2737-2740.

20   J. Ling, C.M. Wallace, J.E.S. Szymanowski and P.C. Burns, *Angew. Chem., Int. Ed.*, 2010, **49**, 7271-7273.

21   K.M. Peruski, V. Bernales, M. Dembowski, H.L. Lobeck, K.L. Pellegrini, G.E. Sigmon, S.M. Hickam, C.M. Wallace, J.E.S. Szymanowski, E. Balboni, L. Gagliardi and P.C. Burns, *Inorg. Chem.*, 2016, **56**, 1333-1339.

22   B.E. Conway, *Amsterdam, Elsevier Scientific Pub. Co. New York*, 1981.

23   M. Nyman, M.A. Rodriguez and C.F. Campana, *Inorg. Chem.*, 2010, **49**, 7748-7755.

24   S.L. Flynn, J.E.S. Szymanowski, Y.Y. Gao, T.B. Liu, P.C. Burns, and J.B. Fein, *Geochim. Cosmochim. Acta*, 2015, **156**, 94-105.

25   Y.Y. Gao, F. Haso, J.E.S. Szymanowski, J. Zhou, L. Hu, P.C. Burns and T.B. Liu, *Chem. – Eur. J.*, 2015, **21**, 18785-18790.

26   D. Gorman-Lewis, J.B. Fein, P.C. Burns, J.E.S. Szymanowski and J. Converse, *J. Chem. Thermodyn.*, 2008, **40**, 980-990.

27   E.J. Sonneveld and J.W. Visser, *J. Appl. Crystallogr.*, 1974, **8**, 1-7.

28   J. Thapa, B. Liu, S.D. Woodruff, B.T. Chorpening and M.P. Buric, *Appl. Opt.*, 2017, **56**, 8598-8606.

29   M. Kadleikova, J. Breza and M. Vesely, *Microelectron. J.*, 2001, **32**, 955-958.

30   M. Ashkin, J.H. Parker and D.W. Feldman, *Solid State Commun.*, 1968, **6**, 343-346.

31   A. Schauer, *Can. J. Phys.*, 1964, **42**, 1857-1864.

32   J.R. Bartlett and R.P. Cooney, *J. Mol. Struct.*, 1989, **193**, 295-300.

33   M. Dembowski, V. Bernales, J.E. Qiu, S. Hickam, G. Gaspar, L. Gagliardi and P.C. Burns, *Inorg. Chem.*, 2017, **56**, 1574-1580.

34   S. Hickam, S.M. Aksenov, M. Dembowski, S.N. Perry, H. Traustason, M. Russell and P.C. Burns, *Inorg. Chem.*, 2018, **57**, 9296-9305.

35   H.L. Lobeck, J.K. Isner and P.C. Burns, *Inorg. Chem.* 2019, Manuscript Submitted.

36   C. Falaise and M. Nyman, *Chem. – Eur. J.*, 2016, **22**, 14678-14687.

37   J. Plasil, *Eur. J. Mineral.*, 2018, **30**, 237-251.

38   A.L. Klingensmith, K.M. Deely, W.S. Kinman, V. Kelly and P.C. Burns, *Am. Mineral.*, 2007, **92**, 662-669.

39   T.A. Olds, J. Plasil, A.R. Kampf, T. Spano, P. Haynes, S.M. Carlson, P.C. Burns, A. Simonetti and O.P. Mills, *Am. Mineral.*, 2018, **103**, 143-150.

40   Q. Liu, Q.C. Zhang, S.L. Yang, H.Q. Zhu, Q.W. Liu and G.X. Tian, *Dalton Trans.*, 2017, **46**, 13180-13187.

41   C. Nguyen-Trung, G.M. Begun and D.A. Palmer, *Inorg. Chem.*, 1992, **31**, 5280-5287.

42   N. Akiya and P.E. Savage, *Chem. Rev.*, 2002, **102**, 2725-2750.

43   J.A. Soltis, C.M. Wallace, R.L. Penn and P.C. Burns, *J. Am. Chem. Soc.*, 2016, **138**, 191-198.

44   M. Sharifironizi, J.E.S. Szymanowski, J. Qiu, S. Castillo, S. Hickam and P.C. Burns, *Inorg. Chem.*, 2018, **57**, 11456-11462.

45   M. Dembowski, C.A. Colla, S. Hickam, A.F. Oliveri, J.E.S. Szymanowski, A.G Oliver, W.H. Casey and P.C. Burns, *Inorg. Chem.*, 2017, **56**, 5478-5487.

46   Y.J. Zhang, M. Bhadbhade, J.R. Price, I. Karatchevtseva, L.G. Kong, N. Scales, G.R. Lumpkin and F. Li, *Polyhedron* 2015, **92**, 99-104.

47   S.M. Tavender, S.A. Johnson, D. Balsom, A.W. Parker and R.H. Bisby, *Laser Chem.*, 1999, **19**, 311-316.

48   R. Wiebe and V.L. Gaddy, *J. Am. Chem. Soc.*, 1940, **62**, 815-817.

49   A.F. Oliveri, C.A. Colla, J.R. Callahan, G. Bogard, J. Qiu, M. Dembowski, P.C. Burns and W.H. Casey, *Eur. J. Inorg. Chem.*, 2017, **46**, 5429-5433.

50   M. Dembowski, C.A. Colla, P. Yu, J. Qiu, J.E.S. Szymanowski, W.H. Casey, and P.C. Burns, *Inorg. Chem.*, 2017, **56**, 9602-9608.

51   M. Nyman and T.M. Alam, *J. Am. Chem. Soc.*, 2012, **134**, 20131-20138.

52   P. Miro, S. Pierrefixe, M. Gicquel, A. Gil and C. Bo, *J. Am. Chem. Soc.*, 2010, **132**, 17787-17794.

53   P. Miro, B. Vlaisavljevich, A. Gil, P.C. Burns, M. Nyman and C. Bo, *Chem. – Eur. J.*, 2016, **22**, 8571-8578.

54   E. Tiferet, A. Gil, C. Bo, T.Y. Shvareva, M. Nyman and A. Navrotsky, *Chem. – Eur. J.*, 2014, **20**, 3646-3651.

55   F. Abraham, B. Arab-Chapelet, M. Rivenet, C. Tamain and S. Grandjean, *Coord. Chem. Rev.*, 2014, **266**, 28-68.

TOC Summary (Max 20 words)

The behaviours of two uranyl peroxide nanoclusters in water heated to 180°C were examined by *in situ* Raman spectroscopy.

TOC Figure